pubs.acs.org/acsaelm Article

Low-Temperature and Ammonia-Free Epitaxy of the GaN/AlGaN/GaN Heterostructure

David Maria Tobaldi,* Valentina Triminì, Arianna Cretì, Mauro Lomascolo, Stefano Dicorato, Maria Losurdo,* Adriana Passaseo, and Vittorianna Tasco

Cite This: *ACS Appl. Electron. Mater.* 2021, 3, 5451−5458

ACCESS | Metrics & More | Article Recommendations

Downloaded via UNIV OF SALENTO on December 3, 2024 at 14:53:45 (UTC).
See https://pubs.acs.org/sharingguidelines for options on how to legitimately share published articles.

ABSTRACT: Wide band-gap semiconductors are very attractive because of their broad applications as electronics and optoelectronics materials, GaN-based materials being by far the most promising. For the production of such nitride-based optical and power devices, metal−organic chemical vapor deposition (MOCVD) is routinely used. However, this has disadvantages, such as the large consumption of ammonia gas and the need for a high growth temperature. To go beyond such a limit, in this study we successfully developed a remote plasma MOCVD (RP-MOCVD) approach for the epitaxial growth of high-quality GaN/AlGaN heterostructures on 4H-SiC substrates. Our RP-MOCVD has the advantages of a lower growth temperature (750 °C) compared to the conventional MOCVD route and the use of a remote N_2/H_2 plasma instead of ammonia for nitrides growth, generating in situ the NH_x (x = 0−3) species needed for the growth. As assessed by structural, morphological, optical, and electrical characterization, the proposed strategy provides an overall cost-effective and green approach for high-quality GaN/AlGaN heteroepitaxy, suitable for high electron mobility transistors (HEMT) technology.

Nitride growth: low temperature (750 °C) & no ammonia

KEYWORDS: *remote plasma MOCVD, ammonia free, low temperature, HEMT, gallium nitride*

1. INTRODUCTION

Group III nitrides have been intensively studied in view of their interesting applications as electronics and optoelectronics components, including light-emitting diodes, laser diodes,[1,2] and high-power/high-frequency high-electron mobility transistors (HEMTs).[3] GaN-based devices, primarily fabricated on foreign substrates because of the lack of high-quality and large-area GaN substrates, exploit the semiconductor technology reference deposition techniques of molecular beam epitaxy (MBE), and metal organic chemical vapor deposition (MOCVD). These techniques are characterized by significant production costs, as they require, respectively, either ultrahigh-vacuum conditions or energy consuming procedures involving high growth temperatures (in the 1000 °C range)[4] and large flows of critical handling gases like ammonia (NH_3). It is thus essential to rethink the aspects of the processes used to make thin films for such technologies to a green and sustainable "*philosophy*", as also recently pointed out by Pedersen et al.[5] Indeed, in recent years, novel approaches have been studied for the synthesis of such materials, allowing, for example, very fast growth rates[6,7] or lower deposition temperatures.[8,9] Among them, plasma technologies represent a high-potential solution for NH_3 replacement with nitrogen, N_2, and nitrogen/hydrogen mixtures, N_2/H_2, and for growth temperature reduction.

In this work, we propose a remote plasma MOCVD (RP-MOCVD) approach, which revealed itself in high-quality, low-temperature growth of a GaN/AlGaN heterostructure on silicon carbide. The peculiarity of our remote plasma (RP) is that only neutrals and electronically excited NH_x (x = 0−3) radicals and N atoms vibrationally excited interact with the growth surface, avoiding ion and electron bombardment, as the substrate is positioned in the plasma afterglow. The presence of the RP source, fed by H_2 and N_2, also grants the advantage of using the low-temperature (200 °C) steps of SiC cleaning and nitridation in situ. This happens before starting the growth at a temperature of 750 °C with plasma-generated NH_x species in situ, instead of ammonia as the nitrogen source. Such a process is an efficient and low-cost means to make a high-quality GaN/AlGaN heterostructure in a more sustainable way

Received: September 22, 2021
Accepted: November 23, 2021
Published: December 4, 2021

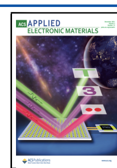

© 2021 American Chemical Society

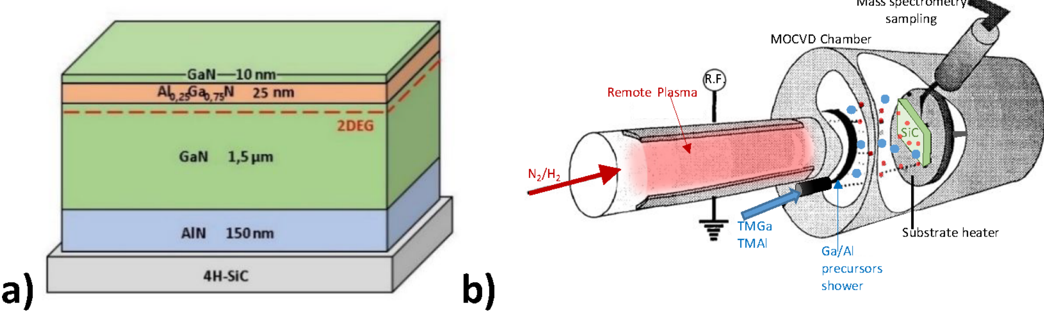

Figure 1. (a) Layout of the GaN/AlGaN/GaN heterostructure grown by RP-MOCVD on 4H-SiC substrate. (b) Schematic of the remote plasma deposition system used to grow the sample.

as compared to conventional semiconductor epitaxial growth techniques, having potential applications in GaN-based electronics.[10−16]

2. METHODS

2.1. Growth of GaN/AlGaN Epilayers. The structure of the sample is reported in Figure 1a: the AlN buffer layer, grown at two different temperatures onto the SiC-4H substrate, is followed by a thick GaN layer (1.5 μm), the AlGaN barrier (25 nm), and a thin GaN cap (10 nm).[17] Sample preparation and growth were performed in the reactor schematically shown in Figure 1b. The 4H-SiC substrate was preliminarily cleaned in situ by an optimized remote H_2 plasma treatment.[12] Subsequently, a SiC nitridation step was run at 200 °C, switching to a remote N_2 plasma to prepare the surface to the AlN nucleation layer.[14] A two-step AlN buffer layer was adopted by first growing a nucleation AlN layer at 200 °C (thickness of about 80 nm) and then increasing the temperature up to 750 °C using a N_2/H_2 plasma and trimethylaluminum (TMA) as the Al precursor. The following GaN/AlGaN/GaN layers of the HEMT heterostructure (Figure 1a) were grown at the same temperature using trimethylgallium (TMG) and trimethylaluminum (TMA) as the gallium and aluminum precursor, respectively, in H_2 carrier gas and in a remote radiofrequency (RF) N_2/H_2 (10% H_2) plasma at a RF power of 200 W and a pressure of 5 Torr. The remote plasma configuration was used to have active dissociated atomic nitrogen species, avoiding radiative and ion bombardment damage of the growing surface. H_2 was also added to react with the N radicals and form in situ the NH_x radicals needed to remove carbon from the growing surface.

2.2. Characterization. The structural properties of the GaN/AlGaN epilayers were examined using high-resolution X-ray diffraction (HR-XRD) performed on a Malvern PanAlytical PW 3050/65 X'pert Pro MRD diffractometer (UK) with Cu Kα radiation. To attain the structural features of the prepared samples, ω−2θ patterns and rocking curves (RC) were recorded in double-axis configuration, in parallel beam mode, using a parabolic mirror and a four-bounce Ge (220) monochromator; the detector was kept at an open detector configuration. Quantitative information about the density of edge (ρ_{edge}) and screw (ρ_{screw}) dislocations in the GaN epilayer was attained by collecting RC along GaN asymmetric and symmetric reflections. To this aim, we employed the rigorous method proposed by Kaganer and colleagues.[18] This assumes the line shape of the X-ray diffraction profiles of the GaN epitaxial layers to be Gaussian only in the central most intense part of the reflection; the tails obey a power law decay, typically proportional to ω^{-3}. To minimize effects due to wafer curvature, the beam height was restricted for symmetric RC, whereas for skew-symmetric ω scans the beam width was restricted, as suggested by Moram and Vickers.[19] X-ray reflectivity (XRR) analysis was performed to obtain information about the thickness of the GaN cap layer. XRR data were modeled with the X'pert Reflectivity software suite. The morphology and the 3-D surface roughness of the samples were investigated by atomic force microscopy (AFM). Characterization of the film topography by AFM was assessed in noncontact mode using the Nanosurf EasyScan atomic force microscope at room temperature (RT), using scan rates of 0.4−2 μm.s^{-1} to obtain 256 × 256 pixel images.

Photoluminescence (PL) measurements were performed as a function of temperature, placing the sample on the coldfinger of a closed cycle helium cryostat, and the temperature was varied from 10 to 300 K. PL was excited with a He−Ag laser operating at 224.3 nm (5.5 eV), and it was recorded through a 0.32 m Triax monochromator and cooled Si-CCD camera. The laser excitation power was varied among 3 orders of magnitude, from 0.5 to 50 mW.

Capacitance−voltage measurements were performed on the as-grown sample using a mercury-probe system (Materials Development Corp., MDC) connected with an Agilent E4980A Precision LCR Meter. Hall measurements were performed by four-point contacts with a Hall EGK HEM-2000 system at RT and at liquid nitrogen temperature.

3. RESULTS AND DISCUSSION

3.1. Structural and Morphological Analyses. In the 2θ−ω scan of the heterostructure, Figure 2a, the (0002) and (0004) reflections of GaN are visible at around 34.5° and 72.8° 2θ, respectively, together with the (0004) and (0008) reflections belonging to the 4H-SiC substrate (at around 35.5° and 75.3° 2θ, respectively). The basal plane of AlN is also recognizable (around 35.9° 2θ). The in-plane epitaxial relationship between the GaN epilayer and the 4H−SiC substrate is further confirmed by the φ scan around the $(10\bar{1}2)$ GaN reflection, as reported in Figure 2b. The results of Kaganer's analysis for GaN symmetric and asymmetric reflections are shown in Figure 2c and 2d, in which the fittings between the observed and the simulated patterns are reported. The insets of Figure 2c and 2d display a log−log scale of simulated and recorded patterns. This is to highlight the tail region in the RCs, which reflects the strain fields in the near vicinity of the dislocation lines. As shown in Figure 2c and 2d, the slope of both the (0002) symmetric and the $(10\bar{1}2)$ asymmetric reflections follows a ω^{-3} asymptotic decay, therefore confirming the scattering from pure screw and edge dislocations, respectively. Average densities of the edge and screw dislocations are 2.90 ± 0.10 × 10^{10} and 0.22 ± 0.04 × 10^{10} cm^{-2}, respectively. The difference between the edge and the screw dislocation density is significant, with ρ_{edge} being much higher than ρ_{screw}; this condition resembles a MBE growth method, which uses a N_2 RF plasma source.[20]

It is interesting to note that the frequently used FWHM method as a measure of the dislocation densities[19] underestimates them as compared to the more rigorous technique proposed by Kaganer. For instance, as also shown in Table 1, with the former we achieve 2.79 × 10^7 and 2.72 × 10^9 cm^{-2} for ρ_{screw} and ρ_{edge}, respectively. Still, this is a lower value

https://doi.org/10.1021/acsaelm.1c00894
ACS Appl. Electron. Mater. 2021, 3, 5451−5458

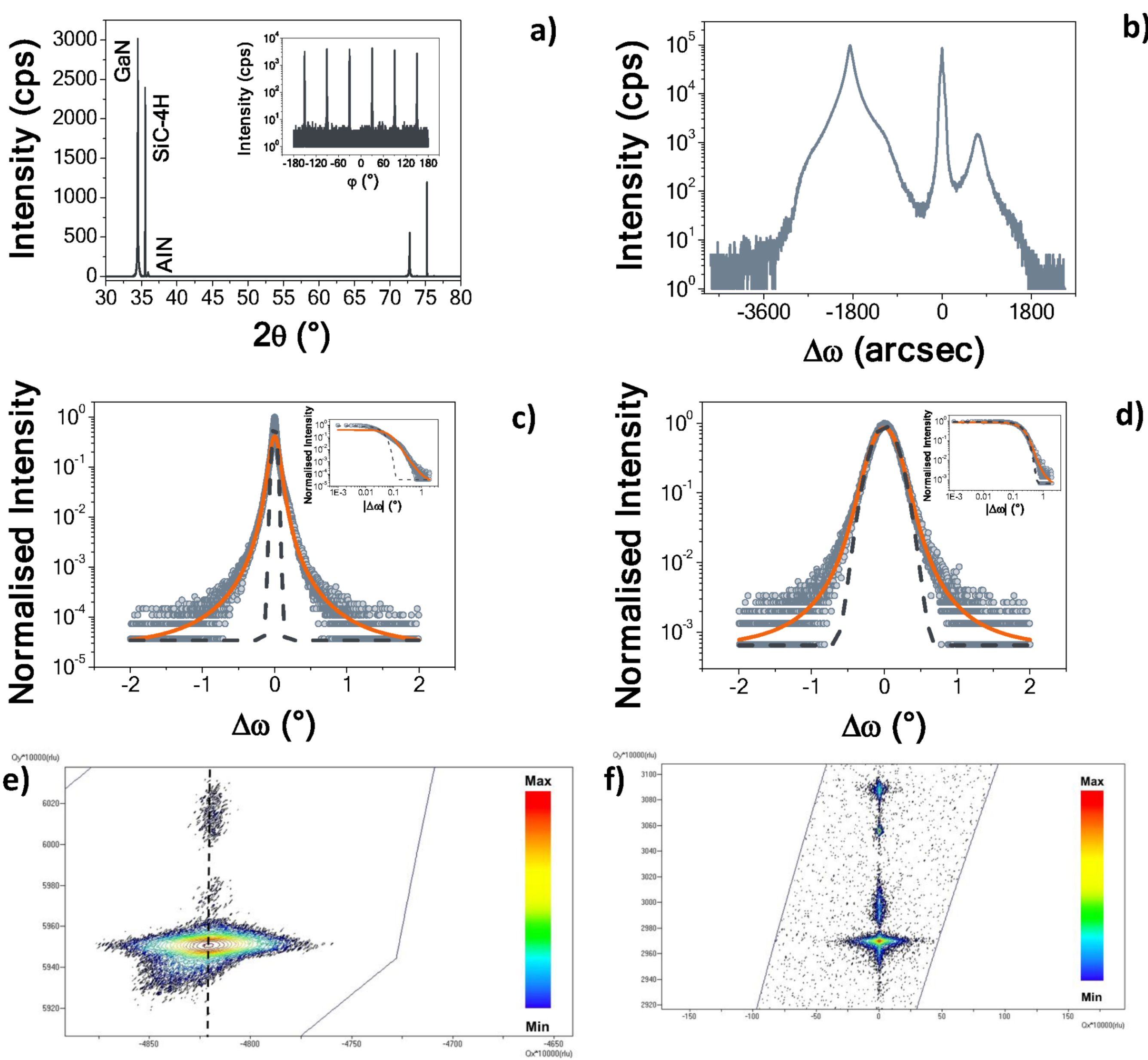

Figure 2. (a) $2\theta-\omega$ scan of the GaN/AlGaN/GaN heterostructure. (Inset) φ scan around the $(10\bar{1}2)$ asymmetric GaN reflection. (b) HRXRD pattern of the sample. (c) Rocking curve, collected with an open detector, from the GaN (0002) symmetric reflection. (Inset) log−log scale profile to show the ω^{-3} asymptotic decay. (d) Rocking curve, collected with an open detector, from the GaN $(10\bar{1}2)$ asymmetric reflection.(Inset) log−log scale profile to show the ω^{-3} asymptotic decay. In c and d, light blue circles are the observed data, continuous orange line the fittings, while black dotted lines represent a Gaussian profile. (e) RSM along the $(\bar{1}\bar{1}24)$ reflection. Vertical dashed line represents the position at which a strained AlGaN epilayer should be. (f) RSM along the (0002) reflection.

Table 1. Dislocation Density in GaN Epitaxial Layer Grown with Conventional Growth Technologies (MOCVD and MBE), as Well as with Different Plasma-Enhanced Growing Methods, Assessed with the FWHM Method and with That Proposed by Kaganer et al.[18] (noted as ref 18)

			ρ_{edge} (cm^{-2})		ρ_{screw} (cm^{-2})		
growth method	thickness (μm)	temperature (°C)	fwhm	ref 18	fwhm	ref 18	ref
MOVPE	4			2.6×10^9		1.5×10^9	20
HVPE	5			4.6×10^{10}		1.6×10^9	20
PAMBE	2.5	690		5.4×10^{10}		5.2×10^8	20
PEALD	0.09	425			3.9×10^7		21
pulsed laser deposition	0.3	750	2.13×10^{10}		6.17×10^9		9
RP-MOCVD	1.5	750	2.72×10^9	2.90×10^{10}	2.79×10^7	2.19×10^9	this work

https://doi.org/10.1021/acsaelm.1c00894
ACS Appl. Electron. Mater. 2021, 3, 5451−5458

compared to the recent literature: on GaN heterostructure, grown via pulsed laser deposition at 750 °C, Wang et al. found ρ_{screw} to be 6.17×10^9 cm^{-2} and $\rho_{edge} = 2.13 \times 10^{10}$ cm^{-2} using the FWHM of the (0002) and $(10\bar{1}2)$ GaN reflections, respectively.[9] The present low values of the dislocation density achieved in our approach are a combination of the use of the remote plasma in all of the steps of the growth, starting from the H_2 plasma cleaning and N_2 plasma nitridation of the substrate to the use of plasma-activated NH_x ($x = 0-3$) for the growth of a two-step AlN buffer layer and GaN/AlGaN at reduced temperature. From the RC fittings, we also obtained the adimensional parameter M that describes the dislocation correlation: the M_{edge} value is much greater than unity (i.e., 20.4 ± 1.9), typical of uncorrelated dislocations.[18] This is also reflected by the high value of characteristic lengths of the dislocation correlations L, which are around 1000 nm.

Reciprocal space maps (RSMs) around the asymmetric $(\bar{1}\bar{1}24)$ and symmetric (0002) reflections were also collected to gain insight on the whole heterostructure (Figure 2e and 2f). In the $(\bar{1}\bar{1}24)$ RSM, the reciprocal lattice points belonging to the AlGaN layer are vertically aligned to those from the underlying GaN (Figure 2e). This means that the AlGaN epilayer is partially relaxed over the GaN buffer layer (the black dashed line in Figure 2e shows where the strained AlGaN epilayer should be). The strained in-plane and out-of-plane unit cell parameters from AlGaN together with those belonging to GaN were also extracted from the RSMs. From these, the values of the in-plane and out-of-plane strain ($\varepsilon_{\parallel}$ and $\varepsilon_{\perp}$) of AlGaN were determined according to the following equations[22]

$$\varepsilon_{\parallel} = \frac{a_{AlGaN} - a_0(x)}{a_0(x)} \quad (1)$$

$$\varepsilon_{\perp} = -2\frac{C_{13}(x)}{C_{33}(x)}\varepsilon_{\parallel} \quad (2)$$

where a_{AlGaN} and $a_0(x)$ are the pseudomorphically strained and bulk in-plane unit cell parameters of AlGaN, respectively, and $C_{13}(x)$ and $C_{33}(x)$ are the AlGaN elastic constants. Their values were determined by means of a linear interpolation between those of bulk GaN and AlN, which were taken from ref 23. The Al concentration x was determined to be 0.24 by means of Vegard's law, thus being consistent with the nominal value of 0.25. From these data, we measured the degree of AlGaN relaxation $r(x)$ according to the method proposed in ref 24, this being 37%. Eventually, knowing $\varepsilon_{\parallel}$, the AlGaN in-plane stress $\sigma_{\parallel}$ can be evaluated using the biaxial modulus Y,[25] with $\varepsilon_{\parallel}$, $\varepsilon_{\perp}$, and $\sigma_{\parallel}$ of the AlGaN strained epilayer being 0.31%, −0.16%, and 1.44 GPa, respectively. The lateral coherence length of the AlGaN epilayer was found, by the X'pert Epitaxy software suite, to be 211 nm, while its mosaic spread was 43 arcsec.

The XRR pattern of the GaN/AlGaN/GaN heterostructure is displayed in Figure 3. From the fitting, the thickness of the GaN cap layer was found to be 11.4 ± 0.1 nm. The technique also allows one to assess the quality of the GaN-cap/AlGaN and AlGaN/GaN interfaces, providing roughness values (RMS) of 0.4 and 0.3 nm, respectively.

The GaN-cap layer RMS, as extracted from the fitting, was 0.7 ± 0.1 nm. The representative AFM image of the GaN/AlGaN/GaN heterostructure grown with RP-MOCVD is shown in Figure 3b, where the presence of pits with a density

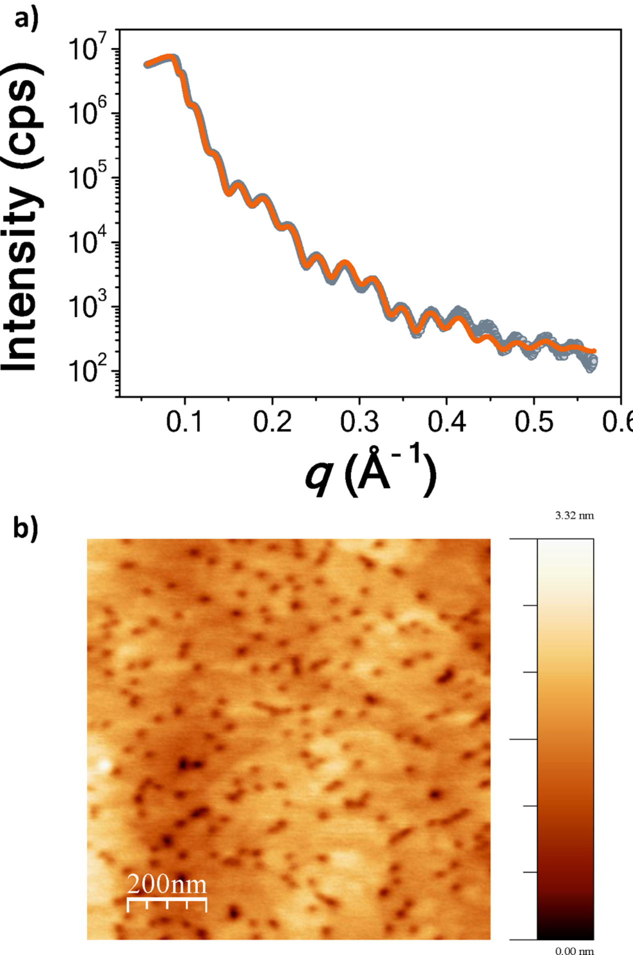

Figure 3. (a) XRR pattern of the GaN/AlGaN/GaN specimen. Full light-blue circles are the observed data; continuous orange line is the calculated data. (b) AFM scan over a 1 μm × 1 μm area.

of around 3.6×10^{10} cm^{-2} can be seen, close to the average dislocation densities resulting from XRD analysis. Yet, the observed pits might be due to current leakage paths associated with open-core screw dislocations, as shown by Kim et al. by means of conductive AFM analyses,[26] or by the methodology proposed by Besendörfer et al.[27] The root-mean-square (RMS) roughness over a 1 μm × 1 μm scanning area is 0.36 nm, thus indicating an overall smooth surface. Atomic steps are also observed, suggesting the onset of a step flow growth mode.

3.2. Optical Characterization. The PL spectrum recorded at RT (Figure 4a) is dominated by the emission signal originating from the GaN layer at about 3.42 eV. At high energy, the contribution of the AlGaN layer is also visible with a narrow emission at 3.88 eV, even though it has a very low intensity. This allows us to estimate the Al concentration value as 23% or 25% according to the model of Nepal et al.[28] or Li et al.,[29] respectively, thus matching the nominal (25%) and experimental value (24% by X-ray analysis) discussed above.

The GaN band-edge PL signal, attributed to excitonic complexes (D^0X, A^0X, etc.) and potentially to 2DEG features, typically expected at low temperature and in the sub-band gap of GaN layer,[30,31] has been investigated by varying the laser power intensity and the sample temperature.

In Figure 4b the PL spectrum, at the maximum excitation power, is reported along with the result of a multi-Gaussian fit performed on the curve, which identifies the contribution of at

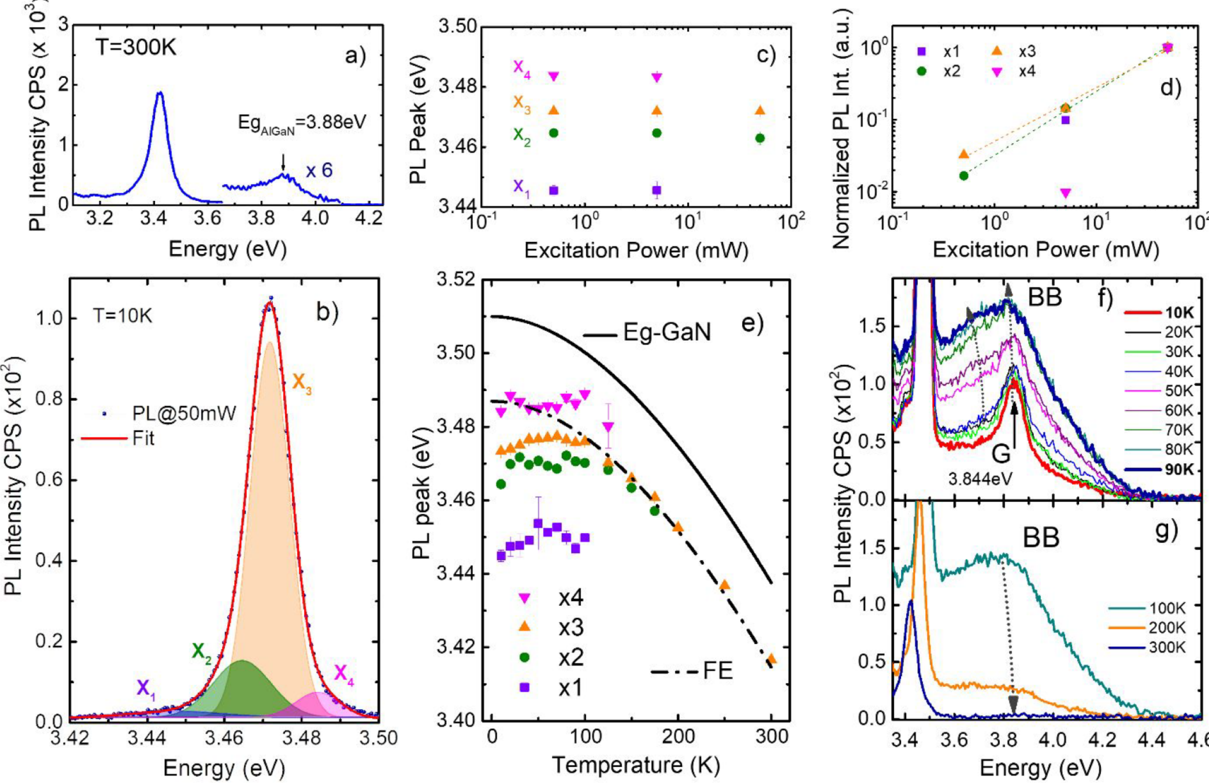

Figure 4. PL analysis of the GaN/AlGaN/GaN sample. (a) RT emission of the structure; peak from AlGaN is magnified ×6. (b) Low-temperature spectrum of the GaN emission, with four bands arising from Gaussian fitting. (c) PL peaks of the x_1, x_2, x_3, and x_4 bands as a function of excitation power. (d) Normalized PL intensity of the x_1, x_2, x_3, and x_4 bands as a function of excitation power. (e) PL peaks of the x_1, x_2, x_3, and x_4 bands as a function of temperature. Theoretical curve for the GaN band gap (continuous black line) and free-exciton ground state (dashed−dotted line) for a binding energy of 23 meV are also shown. (f) PL spectra at high energy as a function of temperature (10−90 K). (g) PL spectra at high energy as a function of temperature (100−300 K).

least 4 sub-bands (x_1, x_2, x_3, and x_4). As a general trend, as the excitation power increases, we observe, for all of the x_i bands, that the energy peak value does not change (Figure 4c) and that the integrated PL intensity increases (Figure 4d). The x_2 and x_3 emission bands show a linear behavior in this power excitation range.

Finally, the x_1 and x_4 emission bands disappear at lower excitation intensity (0.5 mW), and no signature of saturation is present, at least at the maximum power used in the experiments.

Figure 4e shows the temperature dependence of the energy peak values of x_1, x_2, x_3 and x_4. Up to about 100 K, the peak energy of all of the bands blue shifts with increasing temperature, probably due to delocalization effects. At high temperatures, x_1 and x_4 are no longer visible while x_2 and x_3 show the characteristic energy red shift with temperature.[32]

The typical experimental energy values reported in the literature for GaN excitonic complexes in "strained" AlGaN/GaN heterostructures at low temperature[30,31,33] are as follows: ~3.47 eV (A^0X neutral acceptor bound), ~3.48 eV (D^0X neutral donor bound), ~3.49 eV ($FE_{n=1}$ free-exciton ground state), and ~3.51 eV ($FE_{n=2}$ free-exciton excited state). In addition, the 2DEG features (ground and excited states) are reported in a quite wide energy range from 3.44 and 3.47 eV.[30,31,33]

Despite their spectral position, the behavior of the x_1 and x_2 bands, as a function of excitation power, excludes the involvement of the 2DEG states in the recombination process, since there is no blue-shift evidence with increasing excitation power (which could be from a few to hundreds of meV).[31] In addition, the x_2 band can be traced up to ~180 K, well beyond the typical temperature range reported in the literature (40−100 K).[30,31]

The energy of x_3 emission band displays the typical thermal energy red-shift for temperature higher than 100 K, and it follows the theoretical curve of free-exciton recombination − at the assumed binding energy value of 23 meV (Figure 4e, dash-dotted line).[32] Also x_2 seems to follow this trend, although within a narrower temperature range. Therefore, x_2 and x_3 emission bands can be related to the GaN excitonic complex. In particular, x_3 could be ascribed to the FE (ground state), and x_2 to the neutral donor bound exciton (D^0X), which dissociates at high temperature.

Concerning the x_1 band attribution, since there is no clear evidence of 2DEG band emission behavior, as previously discussed, and given its spectral value, we can assume that it originates from a transition involving a neutral acceptor-bound exciton (A^0X). Finally, the small contribution observed at the highest spectral energy (x_4), and from 10 to ~100 K could be due to the free exciton in the first excited state.

It is interesting to note that above the GaN emission, a broad band (BB) is also observed (Figure 4f and 4g) and that, at the lowest temperatures (from 10 to 90 K), a superimposed well-defined narrow band also appears (G). As the temperature increases, the intensity of the G band decreases and, conversely, the BB becomes more and more intense and broadened. For temperatures higher than 100 K, the BB dominates and the G band is no longer distinguishable (Figure

https://doi.org/10.1021/acsaelm.1c00894
ACS Appl. Electron. Mater. 2021, 3, 5451−5458

4f and 4g). The large width of the BB suggests a high trap density in the barrier. Noteworthy, in our experimental conditions (excitation energy is larger than the AlGaN barrier band gap), PL transitions can also originate from recombination of 2DEG electrons and free holes of AlGaN, rather than the free ones at the GaN valence band, resulting in energies higher than the GaN band gap. Free holes from the AlGaN barrier moving to the AlGaN/GaN interface can be trapped (localized holes) and involved in 2DEG transitions.[31,34,35] Therefore, the G band, observed at high energy, which gradually reduces and disappears at 90 K (as expected from transitions involving an electron in the potential well), can be attributed to the 2DEG contribution.

3.3. Electrical Properties. Capacitance−voltage ($C-V$) measurements were performed with the mercury probe to assess the charge profiling in the heterostructure. Figure 5 shows the $C-V$ profile measured at 20 kHz, where one can notice the presence of a capacitance plateau due to the 2D electron gas (2DEG) located at the AlGaN/GaN interface and a pinch off voltage of −6.2 V. A sheet carrier density Ns of the 2DEG of 1.18×10^{13} cm^{-2} is deduced from the measurement. This is consistent with the piezoelectric and spontaneous polarization-induced sheet charge for the pseudomorphically grown AlGaN/GaN heterostructure, as calculated from Ambacher et al.,[24] in the case of conventional growth technologies (MBE and MOCVD). For comparison, we considered the AlGaN barrier having the Al amount and the relaxation value estimated by XRD analysis. The values of the Hall mobility at RT and at low temperature (77 K) are approximately 650 cm^2·V^{-1}·cm^{-1} at RT and 1100 cm^2·V^{-1}·cm^{-1} at 77 K,[36] as listed in the inset of Figure 5, in line with the measured dislocation density.[9]

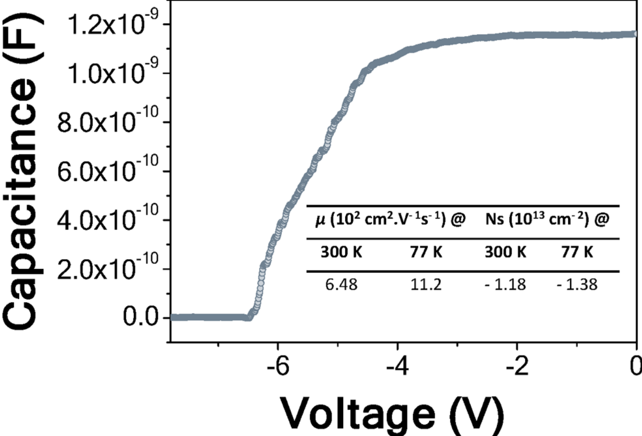

Figure 5. $C-V$ curve acquired by a Hg probe at a frequency of 20 kHz. (Inset) Mobility (μ) and sheet carrier density values (N_s) as obtained by Hall measurements at 300 and 77 K.

4. CONCLUSIONS

The presented data demonstrated that strained GaN/AlGaN heterostructures can be achieved at low temperature (750 °C) with sharp interfaces and an epitaxial relationship among the layers, thus enabling the formation of a 2DEG, which can be used for device applications. The quality of the gallium nitride layer obtained by RP-MOCVD, where the remote plasma is involved in all of the steps of the growth from the in situ SiC substrate cleaning and nitridation, to AlN, GaN, and AlGaN reduced temperature growth meets the state-of-the-art obtained with conventional semiconductor growth technologies (MOCVD and MBE). The plasma configuration chosen is remote with respect to the growth surface, similar to the MBE growth, namely, the substrate is positioned in the plasma afterglow to avoid ion and electron bombardment of the growing front. As a step beyond MBE, in our hybrid approach, the in situ H_2 plasma cleaning of the SiC substrate is integrated in the growth process. As a step beyond conventional MOCVD, we avoid the use of a high flow of NH_3, producing it in situ during the growth with N_2/H_2 plasma activation. For the more critical AlGaN layer, we observe only limited relaxation and a level of strain suitable for the onset of piezoelectric and spontaneous polarization-induced 2DEG with a large carrier density. Optical measurements suggest the presence of defect states in such a layer, which are probably the cause of the still low carrier mobility. The results demonstrate the possibility of achieving HEMT heterostructures without an ammonia source and at low temperature, which can be ascribed to a combination of the substrate preparation steps, engineered buffer layer, and growth conditions.

AUTHOR INFORMATION

Corresponding Authors

David Maria Tobaldi − *Nanotechnology Institute, CNR-Nanotec, Lecce 73100, Italy;* orcid.org/0000-0002-0112-8570; Email: david.tobaldi@nanotec.cnr.it, david@davidtobaldi.org

Maria Losurdo − *Nanotechnology Institute, CNR-Nanotec, Lecce 73100, Italy; Dipartimento di Chimica, Università di Bari, Bari 70126, Italy*; Email: maria.losurdo@cnr.it

Authors

Valentina Triminì − *Nanotechnology Institute, CNR-Nanotec, Lecce 73100, Italy*

Arianna Cretì − *Institute for Microelectronic and Microsystems, CNR-IMM, Lecce 73100, Italy;* orcid.org/0000-0003-0389-660X

Mauro Lomascolo − *Institute for Microelectronic and Microsystems, CNR-IMM, Lecce 73100, Italy*

Stefano Dicorato − *Dipartimento di Chimica, Università di Bari, Bari 70126, Italy*

Adriana Passaseo − *Nanotechnology Institute, CNR-Nanotec, Lecce 73100, Italy*

Vittorianna Tasco − *Nanotechnology Institute, CNR-Nanotec, Lecce 73100, Italy;* orcid.org/0000-0002-3392-0976

Complete contact information is available at: https://pubs.acs.org/10.1021/acsaelm.1c00894

Notes

The authors declare no competing financial interest.

ACKNOWLEDGMENTS

The authors are grateful to the project EleGaNTe−PON ARS01_01007 for funding this research. We thank Prof VM Kaganer, Paul-Drude-Institut für Festkörperelektronik, Berlin (DE), for his helpful and constructive discussions.

REFERENCES

(1) Edmond, J.; Abare, A.; Bergman, M.; Bharathan, J.; Lee Bunker, K.; Emerson, D.; Haberern, K.; Ibbetson, J.; Leung, M.; Russel, P.;

Slater, D. High Efficiency GaN-Based LEDs and Lasers on SiC. *J. Cryst. Growth* **2004**, *272* (1), 242−250.
(2) Jia, C.; Yu, T.; Feng, X.; Wang, K.; Zhang, G. Performance Improvement of GaN-Based near-UV LEDs with InGaN/AlGaN Superlattices Strain Relief Layer and AlGaN Barrier. *Superlattices Microstruct.* **2016**, *97*, 417−423.
(3) Kabemura, T.; Ueda, S.; Kawada, Y.; Horio, K. Enhancement of Breakdown Voltage in AlGaN/GaN HEMTs: Field Plate Plus High-k Passivation Layer and High Acceptor Density in Buffer Layer. *IEEE Trans. Electron Devices* **2018**, *65* (9), 3848−3854.
(4) Tasco, V.; Campa, A.; Tarantini, I.; Passaseo, A.; González-Posada, F.; Redondo-Cubero, A.; Lorenz, K.; Franco, N.; Muñoz, E. Investigation of Different Mechanisms of GaN Growth Induced on AlN and GaN Nucleation Layers. *J. Appl. Phys.* **2009**, *105* (6), No. 063510.
(5) Pedersen, H.; Barry, S. T.; Sundqvist, J. Green CVD—Toward a Sustainable Philosophy for Thin Film Deposition by Chemical Vapor Deposition. *J. Vac. Sci. Technol., A* **2021**, *39* (5), No. 051001.
(6) Cordier, Y.; Damilano, B.; Aing, P.; Chaix, C.; Linez, F.; Tuomisto, F.; Vennéguès, P.; Frayssinet, E.; Lefebvre, D.; Portail, M.; Nemoz, M. GaN Films and GaN/AlGaN Quantum Wells Grown by Plasma Assisted Molecular Beam Epitaxy Using a High Density Radical Source. *J. Cryst. Growth* **2016**, *433*, 165−171.
(7) Rabiee Golgir, H.; Li, D. W.; Keramatnejad, K.; Zou, Q. M.; Xiao, J.; Wang, F.; Jiang, L.; Silvain, J.-F.; Lu, Y. F. Fast Growth of GaN Epilayers via Laser-Assisted Metal−Organic Chemical Vapor Deposition for Ultraviolet Photodetector Applications. *ACS Appl. Mater. Interfaces* **2017**, *9* (25), 21539−21547.
(8) Lu, Y.; Kondo, H.; Ishikawa, K.; Oda, O.; Takeda, K.; Sekine, M.; Amano, H.; Hori, M. Epitaxial Growth of GaN by Radical-Enhanced Metalorganic Chemical Vapor Deposition (REMOCVD) in the Downflow of a Very High Frequency (VHF) N2/H2 Excited Plasma − Effect of TMG Flow Rate and VHF Power. *J. Cryst. Growth* **2014**, *391*, 97−103.
(9) Wang, W.; Yang, W.; Lin, Y.; Zhou, S.; Li, G. Microstructures and Growth Mechanisms of GaN Films Epitaxially Grown on AlN/Si Hetero-Structures by Pulsed Laser Deposition at Different Temperatures. *Sci. Rep.* **2015**, *5* (1), 16453.
(10) Sato, M. Highly Resistive CH-doped GaN Grown by Plasma-assisted Metalorganic Chemical Vapor Deposition. *Appl. Phys. Lett.* **1996**, *68* (7), 935−937.
(11) Tokuda, T.; Wakahara, A.; Noda, S.; Sasaki, A. Substrate Nitridation Effect and Low Temperature Growth of GaN on Sapphire (0 0 0 1) by Plasma-Excited Organometallic Vapor-Phase Epitaxy. *J. Cryst. Growth* **1998**, *183* (1), 62−68.
(12) Losurdo, M.; Bruno, G.; Brown, A.; Kim, T.-H. Study of the Temperature-Dependent Interaction of 4H−SiC and 6H−SiC Surfaces with Atomic Hydrogen. *Appl. Phys. Lett.* **2004**, *84* (20), 4011−4013.
(13) Sugianto, S.; Subagio, A.; Erzam, E.; Sani, R. A.; Budiman, M.; Arifin, P.; Barmawi, M. Epitaxy of GaN Film by Hydrogen Plasma Assisted MOCVD. *J. Math. Fundam. Sci.* **2001**, *33* (1), 1−4.
(14) Losurdo, M.; Giangregorio, M. M.; Bruno, G.; Brown, A.; Kim, T.-H. Study of the Interaction of 4H−SiC and 6H−SiC(0001)Si Surfaces with Atomic Nitrogen. *Appl. Phys. Lett.* **2004**, *85* (18), 4034−4036.
(15) Silie, F.; Junfang, C.; Peng, G.; Chun-ann, W. Stress Analyses of GaN Film Manufactured by ECR Plasma-Enhanced Chemical Vapor Deposition. *Vacuum* **2012**, *86* (10), 1517−1521.
(16) Butcher, K. S. A.; Kemp, B. W.; Hristov, I. B.; Terziyska, P.; Binsted, P. W.; Alexandrov, D. Gallium Nitride Film Growth Using a Plasma Based Migration Enhanced Afterglow Chemical Vapor Deposition System. *Jpn. J. Appl. Phys.* **2012**, *51* (1S), No. 01AF02.
(17) Meneghesso, G.; Rampazzo, F.; Kordos, P.; Verzellesi, G.; Zanoni, E. Current Collapse and High-Electric-Field Reliability of Unpassivated GaN/AlGaN/GaN HEMTs. *IEEE Trans. Electron Devices* **2006**, *53* (12), 2932−2941.
(18) Kaganer, V. M.; Brandt, O.; Trampert, A.; Ploog, K. H. X-Ray Diffraction Peak Profiles from Threading Dislocations in GaN Epitaxial Films. *Phys. Rev. B: Condens. Matter Mater. Phys.* **2005**, *72* (4), No. 045423.
(19) Moram, M. A.; Vickers, M. E. X-Ray Diffraction of III-Nitrides. *Rep. Prog. Phys.* **2009**, *72* (3), No. 036502.
(20) Kaganer, V. M.; Jenichen, B.; Ramsteiner, M.; Jahn, U.; Hauswald, C.; Grosse, F.; Fernández-Garrido, S.; Brandt, O. Quantitative Evaluation of the Broadening of X-Ray Diffraction, Raman, and Photoluminescence Lines by Dislocation-Induced Strain in Heteroepitaxial GaN Films. *J. Phys. D: Appl. Phys.* **2015**, *48* (38), 385105.
(21) Motamedi, P.; Cadien, K. Structure−Property Relationship and Interfacial Phenomena in GaN Grown on C-Plane Sapphire via Plasma-Enhanced Atomic Layer Deposition. *RSC Adv.* **2015**, *5* (71), 57865−57874.
(22) Stanchu, H. V.; Kuchuk, A. V.; Mazur, Y. I.; Li, C.; Lytvyn, P. M.; Schmidbauer, M.; Maidaniuk, Y.; Benamara, M.; Ware, M. E.; Wang, Z. M.; Salamo, G. J. Local Strain and Crystalline Defects in GaN/AlGaN/GaN(0001) Heterostructures Induced by Compositionally Graded AlGaN Buried Layers. *Cryst. Growth Des.* **2019**, *19* (1), 200−210.
(23) Wallis, D. J.; Zhu, D.; Oehler, F.; Westwater, S. P.; Pujol, A.; Humphreys, C. J. Measuring the Composition of AlGaN Layers in GaN Based Structures Grown on 150 Mm Si Substrates Using (2 0 5) Reciprocal Space Maps. *Semicond. Sci. Technol.* **2013**, *28* (9), No. 094006.
(24) Ambacher, O.; Foutz, B.; Smart, J.; Shealy, J. R.; Weimann, N. G.; Chu, K.; Murphy, M.; Sierakowski, A. J.; Schaff, W. J.; Eastman, L. F.; Dimitrov, R.; Mitchell, A.; Stutzmann, M. Two Dimensional Electron Gases Induced by Spontaneous and Piezoelectric Polarization in Undoped and Doped AlGaN/GaN Heterostructures. *J. Appl. Phys.* **2000**, *87* (1), 334−344.
(25) Wagner, J.-M.; Bechstedt, F. Properties of Strained Wurtzite GaN and AlN: *Ab Initio* Studies. *Phys. Rev. B: Condens. Matter Mater. Phys.* **2002**, *66* (11), 115202.
(26) Kim, B.; Moon, D.; Joo, K.; Oh, S.; Lee, Y. K.; Park, Y.; Nanishi, Y.; Yoon, E. Investigation of Leakage Current Paths in N-GaN by Conductive Atomic Force Microscopy. *Appl. Phys. Lett.* **2014**, *104* (10), 102101.
(27) Besendörfer, S.; Meissner, E.; Lesnik, A.; Friedrich, J.; Dadgar, A.; Erlbacher, T. Methodology for the Investigation of Threading Dislocations as a Source of Vertical Leakage in AlGaN/GaN-HEMT Heterostructures for Power Devices. *J. Appl. Phys.* **2019**, *125* (9), No. 095704.
(28) Nepal, N.; Li, J.; Nakarmi, M. L.; Lin, J. Y.; Jiang, H. X. Temperature and Compositional Dependence of the Energy Band Gap of AlGaN Alloys. *Appl. Phys. Lett.* **2005**, *87* (24), 242104.
(29) Li, J.; Nam, K. B.; Lin, J. Y.; Jiang, H. X. Optical and Electrical Properties of Al-Rich AlGaN Alloys. *Appl. Phys. Lett.* **2001**, *79* (20), 3245−3247.
(30) Bergman, J. P.; Lundström, T.; Monemar, B.; Amano, H.; Akasaki, I. Photoluminescence Related to the Two-dimensional Electron Gas at a GaN/AlGaN Heterointerface. *Appl. Phys. Lett.* **1996**, *69* (23), 3456−3458.
(31) Jana, D.; Sharma, T. K. An Unambiguous Identification of 2D Electron Gas Features in the Photoluminescence Spectrum of AlGaN/GaN Heterostructures. *J. Phys. D: Appl. Phys.* **2016**, *49* (26), 265107.
(32) Vurgaftman, I.; Meyer, J. R. Band Parameters for Nitrogen-Containing Semiconductors. *J. Appl. Phys.* **2003**, *94* (6), 3675−3696.
(33) Osinnykh, I. V.; Malin, T. V.; Zhuravlev, K. S. Moving Photoluminescence Band in AlGaN/GaN Heterostructures. *Semicond. Sci. Technol.* **2015**, *30* (8), No. 085010.
(34) Zhang, J.-P.; Sun, D.-Z.; Wang, X.-L.; Kong, M.-Y.; Zeng, Y.-P.; Li, J.-M.; Lin, L.-Y. Fermi-Edge Singularity Observed in a Modulation-Doped AlGaN/GaN Heterostructure. *Appl. Phys. Lett.* **1998**, *73* (17), 2471−2472.
(35) Akopian, N.; Vardi, A.; Bahir, G.; Garber, V.; Ehrenfreund, E.; Gershoni, D.; Poblenz, C.; Elsass, C. R.; Smorchkova, I. P.; Speck, J. S.

Fermi Edge Singularity Observed in GaN/AlGaN Heterointerfaces. *Appl. Phys. Lett.* **2009**, *94* (22), 223502.

(36) Zanato, D.; Gokden, S.; Balkan, N.; Ridley, B. K.; Schaff, W. J. The Effect of Interface-Roughness and Dislocation Scattering on Low Temperature Mobility of 2D Electron Gas in GaN/AlGaN. *Semicond. Sci. Technol.* **2004**, *19* (3), 427−432.

Recommended by ACS

Thermodynamic Origin of High Efficiency in Long-Wavelength InGaN-Based LEDs on Si Substrates

Yu Zhang, Zhihua Xiong, *et al.*

MARCH 20, 2023

THE JOURNAL OF PHYSICAL CHEMISTRY C

READ

Improvement of the Emission Intensity of GaN-Based Micro-Light Emitting Diodes by a Suspended Structure

Yang Mei, Baoping Zhang, *et al.*

NOVEMBER 29, 2022

ACS PHOTONICS

READ

N-AlGaN Free Deep-Ultraviolet Light-Emitting Diode with Transverse Electron Injection

Xingfa Gao, Yun Zhang, *et al.*

FEBRUARY 14, 2023

ACS PHOTONICS

READ

Origin of Surface Barrier Temperature Dependence for the Polar GaN Surface

Ewelina Zdanowicz, Robert Kudrawiec, *et al.*

OCTOBER 04, 2022

ACS APPLIED ELECTRONIC MATERIALS

READ

Get More Suggestions >

https://doi.org/10.1021/acsaelm.1c00894
ACS Appl. Electron. Mater. 2021, 3, 5451−5458